J|A|C|S
ARTICLES
Published on Web 04/24/2007

Solvent Tuning from Normal to Inverted Marcus Region of Intramolecular Electron Transfer in Ferrocene-Based Organic Radicals

Imma Ratera,[†] Christian Sporer,[†] Daniel Ruiz-Molina,[†] Nora Ventosa,[†] Jacob Baggerman,[‡] Albert M. Brouwer,[‡] Concepció Rovira,[†] and Jaume Veciana*,[†]

Contribution from the Institut de Ciència de Materials de Barcelona, Campus Universitari de Ballaterra, 08193 Bellaterra, Catalonia, Spain, and Institute of Molecular Chemistry, University of Amsterdam, Nieuwe Achtergracht 129, NL-1018 WS, Amsterdam, The Netherlands

Received September 1, 2006; E-mail: vecianaj@icmab.es

Abstract: The solvent dependence of spectroscopic data of two neutral paramagnetic donor−acceptor dyads, based on a polychlorinated triphenylmethyl radical acceptor unit linked through a vinylene π-bridge to a ferrocene (compound **1**) or a nonamethylferrocene donor (compound **2**) unit, is described. Both compounds exhibit broad absorptions in the near-IR region, with band maxima appearing around 1000 and 1500 nm for **1** and **2**, respectively. These bands correspond to the excitation of a neutral DA ground state to the charge-separated D^+A^- state, indicative of an intramolecular electron-transfer process. Compounds **1** and **2** show two reversible one-electron redox processes associated with the oxidation of the ferrocene and the reduction of the polychlorotriphenylmethyl radical subunits. The solvent dependence of the redox potentials was also investigated, allowing the determination of the redox asymmetries $\Delta G°$ of both dyads. The latter values, along with the experimental E_{opt} spectroscopic data, allow us to estimate, using the total energy balance $E_{opt} = \lambda + \Delta G°$, the reorganization energy values, λ, and their solvent polarity dependence. Since $\Delta G°$ and λ are of the same order of magnitude but exhibit opposite trends in their solvent polarity dependence, a unique shift from the normal to the inverted Marcus region with the change in solvent polarity is found. The kinetics of the charge recombination step of the excited charge-separated D^+A^- state was studied by picosecond transient absorption spectroscopy, which allows us to observe and monitor for the first time the charge-separated D^+A^- state, thereby confirming unambiguously the photoinduced electron-transfer phenomena.

Introduction

Dyads formed by donor and acceptor units covalently linked by an organic bridge are worthy of attention for the investigation of intramolecular electron-transfer (IET) phenomena.[1] The interest arises from their potential use as molecular wires on integrated molecular-sized devices or for photo-optical, photoconducting, nonlinear optical, or memory applications.[2] Moreover, from the theoretical point of view, such IET studies could give new insights into important natural processes, such as photosynthesis,[3] and also could allow the rules for the prediction and control of electron propagation in molecular wires to be worked out.[4] Up to now, many of the studied mixed-valence compounds exhibiting IET have been homo- and heterodinuclear metallic complexes in which two metal atoms with different oxidation states are connected through an organic bridging ligand. The most famous example of this kind of complexes is the inorganic Creutz−Taube ion.[5] There are also examples of purely organic mixed-valence compounds showing IET based on bishydrazine radicals,[6] polyamines,[7] or tetrathiafulvalenes derivatives,[8] among others.[9,10] Our group is interested in using polychlorotriphenylmethyl (PTM) radicals,[11] which are neutral persistent radicals with excellent electron acceptors abilities, as electron-active centers of mixed-valence compounds.

[†] Campus Universitari de Ballaterra.
[‡] University of Amsterdam.

(1) (a) Harriman, A.; Ziessel, R. *Coord. Chem. Rev.* **1998**, *171*, 331. (b) Paddon-Row, M. N. *Acc. Chem. Res.* **1994**, *27*, 18. (c) Wasielewski, M. R. *Chem. Rev.* **1992**, *92*, 435.
(2) (a) Tour, J. M.; Kozaki, M.; Seminario, J. M. J. *J. Am. Chem. Soc*. **1998**, *120*, 8486. (b) Seminario, J. M., Tour J. M. In *Molecular Electronics—Science and Technology*; Aviram, A., Ratner, M. A., Eds.; New York Academy of Science: New York, 1998; p 69.
(3) Sauvage, J.-P.; Collin, J.-P.; Chambron, J.-C.; Guillerez, S.; Coudret, C. *Chem. Rev.* **1994**, *94*, 993.
(4) (a) Launay, J. P. *Chem. Soc. Rev*. **2001**, *30*, 386−397. (b) Davis, W. B.; Swec, W. A.; Ratner, M. A.; Wasiliewski, M. R. *Nature* **1998**, *396*, 60−63. (c) *Electron Transfer in Chemistry*; Balzani, V., Ed.; Wiley-VCH: Weinheim, 2001.
(5) (a) Creutz, C.; Taube, H. *J. Am. Chem. Soc*. **1969**, *91*, 3988. (b) Creutz, C. *Prog. Inorg. Chem*. **1983**, *30*, 1. (c) Demandis, K. D.; Hartshorn, C. M.; Meyer, T. J. *Chem. Rev*. **2001**, *101*, 2655.
(6) (a) Nelsen, S. F.; Tran, M. A.; Nagy, H. Q. *J. Am. Chem. Soc.* **1998**, *120*, 298. (b) Nelsen, S. F.; Ramm, M. R.; Wolf, J. J.; Powell, D. R. *J. Am. Chem. Soc.* **1997**, *119*, 6863. (c) Nelsen, S. F.; Ismagilov, R. F.; Trieber, D. A. *Science* **1997**, *278*, 846−849.
(7) (a) Bonvoisin, J.; Launay, J. P.; Van der Auweraer, M.; De Schryver, F. C. *J. Phys. Chem*. **1994**, *98*, 5052. (b) Bonvoisin, J.; Launay, J.-P.; Verbouwe, W.; Van der Auweraer, M.; De Schryver, F. C. *J. Phys. Chem*. **1996**, *100*, 17079. (c) Lambert, C.; Nöll, G.; Schelter, J. *Nat. Mater*. **2002**, *1*, 69−73.
(8) (a) Lahlil, K.; Moradpour, A.; Bowlas, C.; Menou, F.; Cassoux, P.; Bonvoisin, J.; Launay, J. P.; Dive, G.; Dehareng, D. *J. Am. Chem. Soc.* **1995**, *117*, 9995. (b) Gautier, N.; Dumur, F.; Lloveras, V.; Vidal-Gancedo, J.; Veciana, J.; Rovira, C.; Hudhomme, P. *Angew. Chem., Int. Ed*. **2003**, *42*, 2765.

Such mixed-valence compounds are composed of a PTM radical unit bridged to its corresponding electron-donating PTM anion through a bridge exhibiting absorptions in the near-infrared (NIR) region associated with IET.[12] On the other hand, such PTM radical acceptor units have also been covalently linked to donor units like ferrocene derivatives to yield asymmetric donor−acceptor dyads which exhibit IET along with *nonlinear* optical,[13] photodimerization,[14] or valence tautomeric properties.[15] One of the most remarkable characteristics of such asymmetric dyads is their reversible redox chemistry, since it allows researchers to "switch on/off" their physical properties by changing their oxidation states by means of an external chemical or electrochemical stimulus.[16] Furthermore, since the PTM radical itself and the oxidized ferrocene are *open-shell* molecules, such compounds also show interesting magnetic properties in combination with IET.

Pioneering theoretical work on IET and charge-transfer (CT) processes, done by Marcus,[17] shows that the energy of an intervalence transition, E_{opt}, is determined by the sum of the energetic asymmetry, $\Delta G°$, between the donor and the acceptor units of the dyad and the reorganization energy, λ, that the system experiences during the charge transfer. Symmetric mixed-valence CT complexes exhibit negligible redox asymmetries due to their symmetric structures, and their CT kinetics are therefore governed by the so-called Marcus-normal region energy conditions, where $\Delta G°$ is smaller than the λ term.[5−8] On the other hand, asymmetric donor−acceptor dyads usually exhibit large redox asymmetries, which place them in the Marcus-inverted region, with $\Delta G°$ values larger than λ.[9,10] In this particular region, the CT process occurs via a different kinetic pathway, and unusual features associated with the environment of dyads are quite common.[17,18] Although it is known that solvent effects can influence strongly the relative values of $\Delta G°$ and λ terms in the context of IET in proteins and other biological environment,[19] as far as we know, there is no previous example of a molecule that can be shifted from the Marcus-normal to the inverted region simply by changing the polarity of the solvent.

Scheme 1

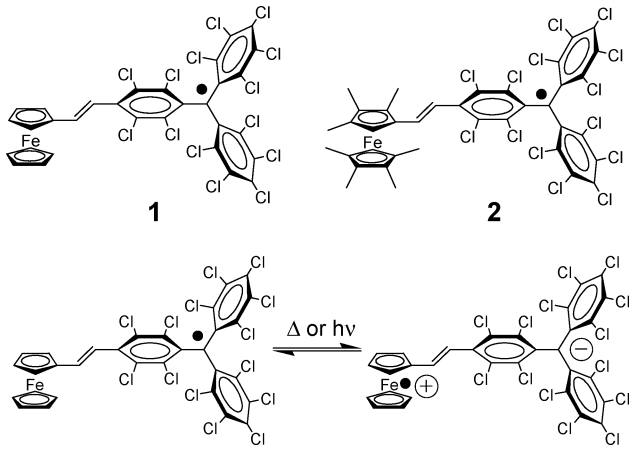

Here we report the first observation of donor−acceptor dyads that can be tuned from the normal to the inverted Marcus region simply by changing the nature of the solvent, because the redox asymmetry and the reorganization energy of such dyads are of similar magnitudes and small changes in the environment can modify such energies. This fact is of utmost importance in the field of molecular electronics, since striking differences in the electron transport mechanism of a molecule just due to its environment are indicated. This result may also have important implications in the mechanism of an IET of single molecules when they are deposited, for example, on a surface. The molecules subject to study are the novel ferrocene−vinylene−PTM dyad **1** and the nonamethylferrocene−vinylene−PTM dyad **2**. Both compounds consist of an acceptor unit and a donor unit, which both may exist in two different oxidation states, linked by a vinylene bridge that mediates the intramolecular electron transfer from one site to the other under the effect of external thermal or optical stimulii (Scheme 1).

Donor−acceptor dyads like **1** and **2** are of particular interest with regard to the study of thermally induced IET phenomena and photoinduced charge separation,[20] since the redox potential of the donor unit and, therefore, the energetic asymmetry must be different because of the distinct substituents (H atoms and methyl groups) in the ferrocenyl unit. Moreover, compounds **1** and **2** are good candidates for such studies, since IET phenomena can be monitored easily by the study of the intervalence transition or CT bands in the NIR region of the spectra.

(9) (a) Utamapanya, S.; Rajca, A. *J. Am. Chem. Soc.* **1991**, *113*, 9242. (b) Telo, J. P.; Shohoji, C. B. L.; Herold, B.; Grampp, G. *J. Chem. Soc., Faraday Trans.* **1992**, *88*, 47. (c) Hviid, L.; Brouwer, A. M.; Paddon-Row, M. N.; Verhoeven, J. W. *Chem. Phys. Chem*. **2001**, *2*, 232. (d) Jolliffe, K. A.; Bell, T. D. M.; Ghiggino, K. P.; Langford, S. J.; Paddon-Row, M. N. *Angew. Chem., Int. Ed*. **1998**, *37*, 916. (e) Bell, T. D. M.; Ghiggino, K. P.; Jolliffe, K. A.; Ranasinghe, M. G.; Langford, S. J.; Shephard, M. J.; Paddon-Row, M. N. *J. Phys. Chem. A* **2002**, *106*, 10079. (f) Sandanayaka, A. S. D.; Sasabe, H.; Araki, Y.; Furusho, Y.; Ito, O.; Takata, T. *J. Phys. Chem. A* **2004**, *108*, 5145.

(10) (a) Closs, G. L.; Miller, J. R. *Science* **1988**, *240*, 440. (b) Closs, G. L.; Calcaterra, L. T.; Green, N. J.; Penfield, K. W.; Miller, J. R. *J. Phys. Chem.* **1986**, *90*, 3673. (c) Miller, J. R.; Calcaterra, L. T.; Closs, G. L. *J. Am. Chem. Soc*. **1984**, *106*, 3047.

(11) (a) Ballester, M.; Riera, J.; Castaner, J.; Rodriguez, A. *Tetrahedron Lett.* **1971**, *2079*. (b) Ballester, M.; Riera, J.; Castaner, J.; Veciana, J.; Rovira, C. *J. Org. Chem*. **1982**, *47*, 4498. (c) Ballester, M. *Acc. Chem. Res*. **1985**, *297*, 131. (d) Veciana, J.; Riera, J.; Castaner, J.; Ferrer, N. *J. Organomet. Chem.* **1985**, *297*, 131. (e) Armet, O.; Veciana, J.; Rovira, C.; Riera, J.; Castaner, J.; Molins, E.; Rius, J.; Miravitlles, C.; Olivella, S.; Brichfeus, J. *J. Phys. Chem*. **1987**, *91*, 5608 and references cited therein.

(12) (a) Bonvoisin, J.; Launay, J. P.; Rovira, C.; Veciana, J. *Angew. Chem., Int. Ed. Engl*. **1994**, *33*, 2106. (b) Rovira, C.; Ruiz-Molina, D.; Elsner, O.; Vidal-Gancedo, J.; Bonvoisin, J.; Launay, J-P.; Veciana, J. *Chem. Eur. J*. **2001**, *7*, 240. (c) Ballester, M.; Pascual, I.; Riera, J.; Castaner, J. *J. Org. Chem*. **1991**, *56*, 217. (d) Sedó, J.; Ruiz-Molina, D.; Vidal-Gancedo, J.; Rovira, C.; Bonvoisin, J.; Launay, J-P.; Veciana, *J. Adv. Mater*. **1996**, *8*, 748.

(13) (a) Ratera, I.; Ruiz-Molina, D.; Sánchez, C.; Alcalà, R.; Rovira, C.; Veciana, J. *Synth. Met.* **2001**, *121*, 1834. (b) Ratera, I.; Létard, J.-F.; Marcén, S.; Ruiz-Molina, D.; Freysz, E.; Rovira, C.; Veciana, J. *Chem. Phys. Lett.* **2002**, *363*, 245. (c) Ratera, I.; Ruiz-Molina, D.; Sporer, C.; Marcen, S.; Létard, J.-F.; Freysz, E.; Rovira, C.; Veciana, J. *Polyhedron* **2003**, *22*, 1851−1856.

(14) (a) Ratera, I.; Ruiz-Molina, D.; Vidal-Gancedo, J.; Wurst, K.; Daro, N.; Létard, J.-F.; Rovira, C.; Veciana, J. *Angew. Chem., Int. Ed*. **2001**, *40*, 919. (b) Ratera, I.; Ruiz-Molina, D.; Vidal-Gancedo, J.; Novoa, J.; Wurst, K.; Létard, J.-F.; Rovira, C.; Veciana, J. *Chem. Eur. J.* **2004**, *10*, 603.

(15) Ratera, I.; Ruiz-Molina, D.; Renz, F.; Ensling, J.; Wurst, K.; Rovira, C.; Gütlich, P.; Veciana, J. *J. Am. Chem. Soc.* **2003**, *124*, 6794.

(16) (a) Sporer, C.; Ratera, I.; Ruiz-Molina, D.; Zhao, Y.; Wurst, K.; Jaitner, P.; Vidal-Gancedo, J.; Clays, K.; Persoons, P.; Rovira, C.; Veciana, J. *Angew. Chem., Int. Ed.* **2004**, *43*, 5266. (b) Sporer, C.; Ratera, I.; Wurst, K.; Vidal-Gancedo, J.; Ruiz-Molina, D.; Rovira, C.; Veciana, J. *Arkivoc* **2005**, (ix), 104.

(17) (a) Marcus, R. A. *J. Chem. Phys.* **1956**, *24*, 966. (b) Marcus, R. A. *Annu. Rev. Phys. Chem*. **1964**, *15*, 155. (c) Marcus, R. A.; Sutin, N. *Biochim. Biophys. Acta* **1985**, *811*, 265.

(18) Chen, P.; Meyer, T. J. *Chem. Rev*. **1998**, *98*, 1439−1477.

(19) (a) Kriegl, J. M.; Ulrich Nienhaus, G. *Proc. Natl. Acad. Sci. U.S.A.* **2004**, *101*, 123. (b) Cascella, M.; Magistrato, A.; Tavernelli, I.; Carloni, P.; Rothlisberger, U. *Proc. Natl. Acad. Sci. U.S.A.* **2006**, *103*, 19641. (c) Warshel, A.; Chu, Z. T.; Parson, W. W. *Science* **1989**, *246*, 112.

(20) (a) Gust, D.; Moore, T. A.; Moore, A. L. *Acc. Chem. Res.* **1993**, *26*, 198. (b) Harriman, A.; Sauvage, J.-P. *Chem. Soc. Rev.* **1996**, *25*, 41. (c) Gust, D.; Moore, T. A.; Morre, A. L.; Lee, S. L.; Bittersmann, E.; Luttrull, D. K.; Rehms, A. A.; DeGraxiano, J. M.; Ma, X. C.; Gao, F.; Belford, R. E.; Trier, T. T. *Science* **1990**, *248*, 199.

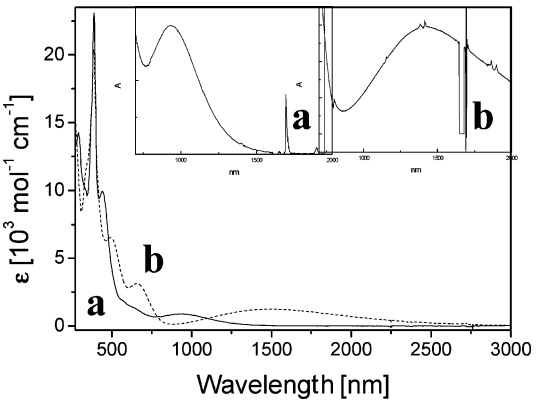

Figure 1. UV−vis−NIR spectra of radicals **1** (a) and **2** (b) in dichloromethane. Insets show the CT bands of both dyads.

Experimental Section

Synthesis. The synthesis and structures of donor−acceptor dyads **1** and **2** have been described elsewhere.[12b,16,21]

Optical Spectroscopy. All solvents were super purity grade from Romil Chemical Co. and were distilled before use. All reagents, organic and inorganic, were of high purity grade and obtained from E. Merck, Fluka Chemie, and Aldrich Chemical Co. UV−visible and NIR spectra were recorded using a Varian Cary 05E spectrophotometer. Time-resolved absorption spectra were recorded using a femtosecond transient absorption setup which has been described elsewhere.[22] Briefly, an amplified Ti:sapphire laser system (Spectra-Physics Hurricane) equipped with an optical parametric amplifier was used to produce a train of ca. 100 fs laser pulses at a repetition rate of 1 kHz. The probe beam was provided by white light generated by focusing a small amount (20 μJ/pulse) of the fundamental beam (800 nm) on a sapphire plate or on a stirred 2 mm H_2O cell. The probe beam was then focused on the sample, which was contained in a cyclindrical cuvette (path length 1 mm) that was rotating about an axis parallel to the excitation beam. The transmitted light was coupled to the detectors by optical fibers. An Ocean Optics (Si, 2048 px) plug-in card diode array was used for the UV−vis region (200−1100 nm), and a Control Development Inc. (InGaAs, 256 px) plug-in card diode array was used for the NIR region (900−1700 nm). In order to probe a homogeneously excited area, the pump beam was focused to an area of ~0.25 mm^2, and the probing area was kept to ~0.1 mm^2.

Electrochemistry. Cyclic voltammograms were recorded with conventional three-electrode equipment from EG&G Princeton Applied Research with Pt electrodes and a Ag/AgCl reference at 298 K. Scan rates were 100 or 200 mV/s. Solvents were purified by distillation over appropriate drying agents under an argon atmosphere and filtered over basic alumina. *n*-Tetrabutylammonium hexafluorophosphate ((TBA)-PF_6) was used as supporting electrolyte.

Results and Discussion

1. Optical Spectroscopy. 1.1. UV−Vis Spectra. PTM radicals usually show an intense absorption band at 387 nm and several weaker bands centered between 565 and 605 nm, all of which are assigned to the radical character of the triphenylmethyl units.[11e] The absorption spectra of radicals **1** and **2** (Figure 1) also show the intense radical absorption at 387 nm, along with two partially unresolved and weak bands centered at 442 and 500 nm for **1** and at 497 and 650 nm for **2**. The two lower energy absorptions observed in both radicals are unprecedented for nonconjugated PTM radicals and are therefore ascribed to the electronic conjugation of the unpaired electrons into the π-framework of the unsaturated substituents at the para position, i.e., specifically to a π-bridge-to-PTM acceptor CT band, as found for other π-conjugated PTM radicals. Other origins of such absorptions might be a Fe(dπ) → Cp(π*) metal-to-ligand-bridge charge-transfer (MLCT) band or a d−d transition, characteristic of the ferrocene units. However, since the absorptions around 500 nm for radical **1** and at 650 nm for radical **2** nm show a large positive solvatochromism and an increasing intensity with solvent polarity, these bands most likely correspond to π-bridge-to-PTM acceptor CT absorptions.[23,24] (See also the Supporting Information for a more detailed argument for this assignment.)

1.2. Near-IR Spectra. More interesting is the observation of intense broad bands in the NIR region for radicals **1** and **2**, with maxima around 1000 and 1500 nm, respectively. Such bands are unprecedented for both conjugated and nonconjugated PTM radicals as well as for ferrocenyl derivatives, and therefore they are assigned to the IET process from the ferrocene unit (donor) to the radical unit (acceptor). In support of such an assignment is the concentration dependence of these CT bands that follows the Beer−Lambert law, confirming that the electron transfer should have an intramolecular character rather than an intermolecular one. Similar CT transitions with equal low-energy absorption bands have already been observed for ferrocenylpyridine and rutheniumamine derivatives in which the ferrocenyl units act as donors and the N-based ligands as acceptor units.[25] A few other related examples of PTM-based donor−acceptor dyads also show similar CT transitions in the NIR region.[16,26]

The excellent solubility of radicals **1** and **2** has allowed us to study in detail the solvent dependence of their CT absorptions in a broad range of 22 common organic solvents, from apolar solvents, like *n*-hexane, to polar solvents, like acetonitrile and dimethylsulfoxide (DMSO), including also protic polar solvents, such as EtOH (Figure 2 and Tables 1 and 2).

As shown in Figure 2 for a few selected solvents, their nature influences dramatically both the band shape and the exact position of the maximum of the CT absorption. Thus, for radical **1**, the position of the band maxima varies from 892 nm in *n*-hexane to 1003 nm in DMSO ($\Delta\lambda$ = 113 nm; $\Delta\tilde{\nu}$ = 1260 cm^{-1} or 0.15 eV), indicating a positive solvatochromism where the charge-separated excited state is more stabilized with respect the neutral ground state in polar solvents. Such a positive solvatochromism is even larger for radical **2**, as evidenced by the position of the CT band maxima observed in *n*-hexane, 1371 nm, and in nitrobenzene, 1726 nm ($\Delta\lambda$ = 346 nm; $\Delta\tilde{\nu}$ = 1540 cm^{-1} or 0.18 eV). The solvatochromism of compound **2** is found to be one of the largest described in the literature for these kinds of compounds. Generally, for both compounds, the CT absorp-

(21) Elsner, O.; Ruiz-Molina, D.; Vidal-Gancedo J.; Rovira, C.; Veciana, J. *Chem. Commun.* **1999**, 579.
(22) Cecchetto, E.; Slooff, L. H.; De Cola, L.; Zhang, H. *J. Lumin.* **2007**, *122*−*123*, 546.
(23) The exact assignment of the bands is possible considering solvatochromic and electrochemical data obtained in different solvents and the orbital energy scheme of Model 3 described by Barlow et al.; see ref 24 and the Supporting Information.
(24) (a) Barlow, S.; Bunting, H. E.; Ringham, C.; Green, J. C.; Bublitz, G. U.; Boxer, S. G.; Perry, J. W.; Marder, S. R. *J. Am. Chem. Soc.* **1999**, *121*, 3715. (b) Johnson, R. C.; Hupp, J. T. *J. Am Chem. Soc.* **2001**, *123*, 2053.
(25) (a) Liu, T.-Y.; Chen, Y. J.; Tai, C.-C.; Kwan, K. S. *Inorg. Chem.* **1999**, *38*, 674. (b) Chen, Y. J.; Kao, C.-H.; Lin, S. J.; Tai, C.-C.; Kwan, K. S. *Inorg. Chem.* **2000**, *39*, 189.
(26) (a) Sporer, C.; Ratera, I.; Ruiz-Molina, D.; Vidal-Gancedo, J.; Wurst, K.; Jaitner, P.; Rovira, C.; Veciana, J. *J. Phys. Chem. Solids* **2003**, *65*, 753. (b) Heckmann, A.; Lambert, C.; Goebel, M.; Wortmann, R. *Angew. Chem., Int. Ed.* **2004**, *43*, 5851.

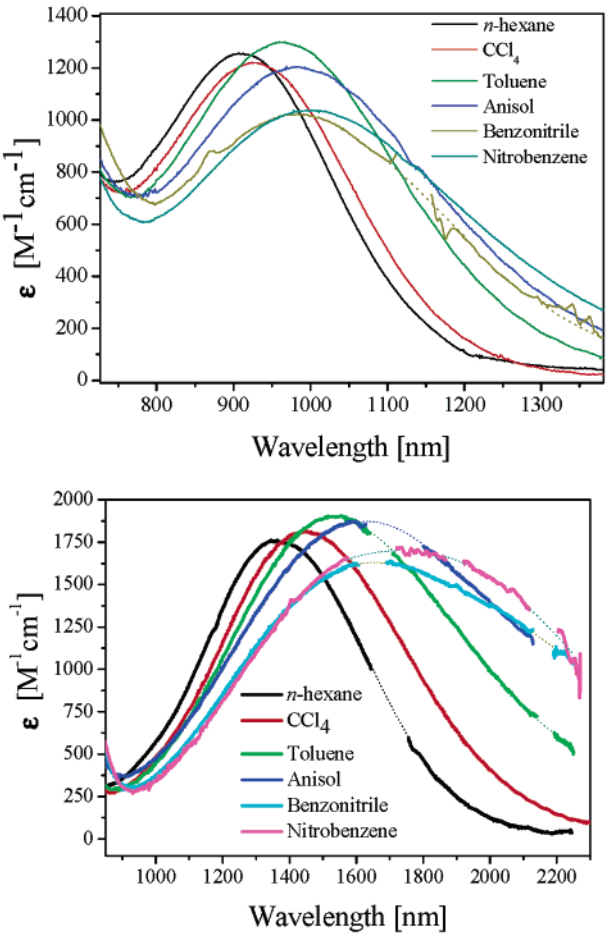

Figure 2. Charge-transfer bands of compounds **1** (top) and **2** (bottom) in some selected solvents. Dashed lines represent best fits in spectral ranges in which solvent artifacts are present.

Table 1. Spectral Data for Charge-Transfer Bands and Coupling Parameters of Dyad **1** in Various Solvents

solvent	λ_{max} (nm)	$\tilde{\nu}_{max}$ (cm^{-1})	ϵ_{max} (M^{-1} cm^{-1})	$\Delta\tilde{\nu}_{1/2}$ (cm^{-1})	H_{AB}[a] (cm^{-1})
1. *n*-hexane	891	11220	1200	3010	436
2. cyclohexane	912	10960	1250	2920	434
3. benzene	961	10400	1230	3400	452
4. CCl_4	928	10780	1210	2980	428
5. 1,4-dioxane	934	10710	1140	3520	450
6. toluene	964	10370	1300	3300	457
7. anisol	984	10160	1210	3680	461
8. 1,2-dibromoethane	962	10390	1190	3550	455
9. chloroform	926	10800	1010	3600	429
10. diethyl ether	936	10680	1130	3680	456
11. chlorobenzene	974	10270	1180	3780	465
12. ethyl acetate	947	10550	1080	3960	460
13. THF	969	10310	1130	3890	461
14. dichloromethane	940	10640	1040	3800	443
15. *tert*-butanol	944	10590	1130	3670	453
16. benzonitrile	982	10180	1020	3890	435
17. nitrobenzene	1004	9960	1040	3910	436
18. DMSO	1001	9980	1150	4420	488
19. acetone	951	10510	1040	4200	465
20. DMF	991	10090	1120	4280	476
21. ethanol	965	10360	1160	4010	476
22. acetonitrile	927	10790	1130	4610	513

[a] Coupling parameters were calculated with eq 1 using r_{DA} = 9.5 Å.

tions are found to have higher intensities in apolar solvents, while they tend to be broader and less intense in polar solvents.

Table 2. Spectral Data for Charge-Transfer Bands and Coupling Parameters of Dyad **2** in Various Solvents

solvent	λ_{max} (nm)	$\tilde{\nu}_{max}$ (cm^{-1})	ϵ_{max} (M^{-1} cm^{-1})	$\Delta\tilde{\nu}_{1/2}$ (cm^{-1})	H_{AB}[a] (cm^{-1})
1. *n*-hexane	1363	7340	1760	3170	429
2. cyclohexane	1395	7170	1790	3170	428
3. benzene	1541	6490	1920	3570	447
4. CCl_4	1450	6900	1870	3260	435
5. 1,4-dioxane	1445	6920	1260	4250	408
6. toluene	1533	6520	1750	3800	442
7. anisol	1608	6220	1840	3880	447
8. 1,2-dibromoethane	1522	6570	1770	3780	445
9. chloroform	1410	7090	1470	4430	455
11. chlorobenzene	1606	6230	1850	3990	455
12. ethyl acetate	1526	6550	1550	4320	444
13. THF	1531	6530	1530	4530	452
14. dichloromethane	1476	6770	1440	4400	439
16. benzonitrile	1651	6060	1620	4590	450
17. nitrobenzene	1723	5800	1750	4280	442
19. acetone	1517	6590	1370	5200	459

[a] Coupling parameters were calculated with eq 1 using r_{DA} = 9.7 Å.

From the experimental spectra, four different parameters have been measured or evaluated in order to characterize the CT absorptions associated with the IET process: (1) the wavelength of the maximum, λ_{max} (in nm), or its associated energy, $\tilde{\nu}_{max}$ (in cm^{-1}), also named E_{opt}; (2) the bandwidth at half-height of the CT band, $\Delta\tilde{\nu}_{1/2}$ (in cm^{-1}); (3) the molar absorption coefficient of the band, ϵ_{max} (in M^{-1} cm^{-1}); and (4) the donor−acceptor coupling parameter, H_{AB} (in cm^{-1}), which measures the electronic interaction between the two units and can be obtained from the previous three spectral parameters with eq 1.[27] The resulting data for all studied solvents are given in Tables 1 and 2.[28,29]

It is also worth nothing that the replacement of the H atoms of the ferrocene unit by CH_3 groups has a dramatic impact on the energy of the IET, since the corresponding absorptions are strongly red-shifted by several hundreds of nanometers; e.g., in dichloromethane the CT bands appear at 940 and 1476 nm for compounds **1** and **2**, respectively. Such an effect clearly arises from the enhanced donor character of the methylated ferrocene moiety. Another interesting result is that the molar absorption coefficients found for the radical band appearing at 387 nm for dyad **2** (ϵ = 23 500 M^{-1} cm^{-1}) in any solvent is always smaller than that exhibited by dyad **1** (ϵ = 26 500 M^{-1} cm^{-1}), while the intensities of the ferrocene donor-to-PTM acceptor and the bridge-to-PTM acceptor CT absorptions are higher for **2** (see Figure 1). This intensity reversal is an indication of a higher degree of charge delocalization in compound **2** than in **1** due to the high electron donor ability of its ferrocene unit, which induces a decrease in the radical character at the expense of a higher degree of charge separation (see Scheme 1).

2. Donor−Acceptor Coupling Strengths. The classical CT theory, developed by Marcus and Hush, provides a simple basis for the description of IET processes in dyads **1** and **2**.[17,30] According to this theory, the adiabatic potential energy surfaces

(27) (a) Crutchley, R. J. *Adv. Inorg. Chem.* **1994**, *41*, 273. (b) Creutz, C. *Prog. Inorg. Chem.* **1983**, *30*, 1.
(28) In order to calculate exactly such experimental parameters, some simulations of such absorption bands have been performed by using the TableCurve Software.
(29) For all the band shape analysis, an epsilon vs wavenumber [cm^{-1}] representation of the absorption spectra has to be used, since in this way a linear relationship with the energy is obtained.

Scheme 2

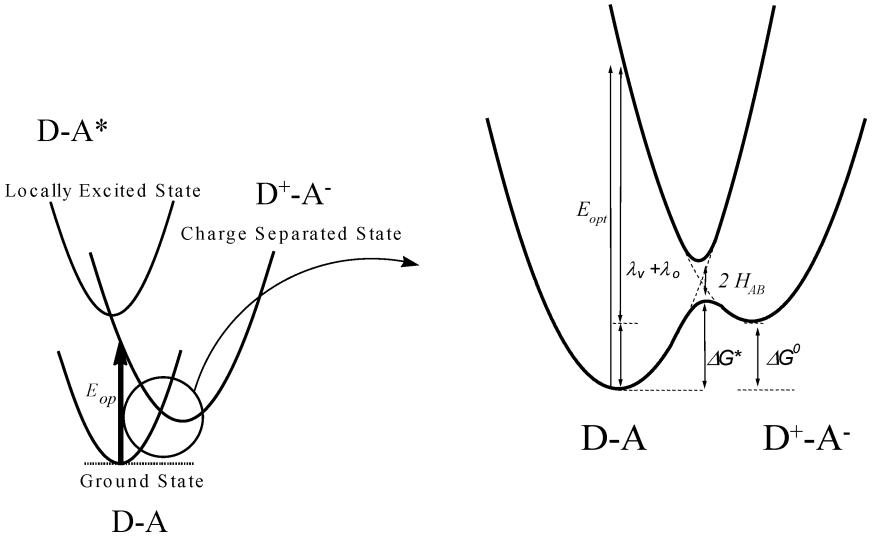

for the reactant (the DA ground state) and the product (the D^+A^- charge-separated state) can be constructed from two parabolic functions, which represent the diabatic (non-interacting) states, taking into account the electronic coupling energy H_{AB} between the two states (see Scheme 2). Charge transfer from the neutral DA ground state to the excited D^+A^- charge-separated one can occur either via a thermally induced process, when the thermal energy is high enough to cross the activation energy barrier, ΔG^*, or via an optically induced process. The latter process can either occur through the population of a locally excited (D−A)* state, which rapidly decays to the D^+A^- state, or proceed directly to this excited charge-separated state.[30d,31b]

Following the theory of Mulliken and Hush,[31] the energy of the electronic interaction between the donor and the acceptor units of a donor−acceptor dyad can be calculated from the band shape parameters of the corresponding CT absorption band. It consists of a *two-state model* where it is assumed that a charge recombination occurs between the ground states of the charge-separated state and the neutral state rather than from vibrational excited states. In this case, the CT absorption band has a Gaussian shape, and the electronic donor-to-acceptor coupling parameter H_{AB} (in cm^{-1}) can be calculated by the following simple expression,

$$H_{AB} = (2.05 \times 10^{-2}) \frac{[\epsilon_{max}\, \Delta\tilde{\nu}_{1/2}\, \tilde{\nu}_{max}]^{1/2}}{r_{DA}} \qquad (1)$$

where $\Delta\tilde{\nu}_{1/2}$ (in cm^{-1}) is the bandwidth at half-height of the CT band maximum, $\tilde{\nu}_{max}$ (in cm^{-1}) is the CT band maximum, which is the energy of the CT absorption, ϵ_{max} is the molar absorptivity (in $M^{-1}\ cm^{-1}$) of the CT band maximum, and r_{DA} (in Å) is the distance between the opposite charges in the charge-separated D^+A^- excited state. A common way to estimate the CT separation r_{DA} is to use crystallographic data, assuming that charges are totally localized on two atomic sites of the dyad, which in our case are the central sp^2-hybridized carbon atom of the PTM radical unit and the Fe atom of the ferrocene unit. Such a distance is estimated to be 9.5 and 9.7 Å from the crystallographic data for compounds **1** and **2**, respectively.[15,16] A distance identical to that for radical **1** has also been found for the reduced anionic derivative $\mathbf{1}^-$ from its crystallographic data.[16b] Although no crystallographic data are available for the cationic species $\mathbf{1}^+$ or $\mathbf{2}^+$, derived from **1** and **2**, nor for the reduced species $\mathbf{2}^-$, changes in the molecular geometries are expected to be small. However, it is known from Stark spectroscopic experiments that the effective CT distances of donor−acceptor dyads are usually much smaller due to a charge delocalization over the molecule and a non-negligible dipole moment in the molecule ground state.[24] Thereby, the coupling parameters H_{AB} calculated from the crystallographic data are underestimated and should always be considered only as the lower limit of the actual values.

Equation 1 was deduced assuming symmetrical Gaussian-type absorption CT bands, but as can be clearly seen in Figure 2, this is not the case for compounds **1** and **2**, where the bands are slightly asymmetric, showing a steeper fall-off for the low-energy side of the band than for the higher energy side.[32] However, since both compounds exhibit moderate coupling strengths, which places them in the Robin−Day Class II,[33] considering the absorption bands as symmetric Gaussian bands gives rise to small errors. Thus, we have measured the $\Delta\tilde{\nu}_{1/2}$ values directly from the CT bands of the NIR spectra for compound **2**. For the CT band of compound **1**, the overlap with other higher energy absorptions forced us to make a spectral deconvolution using two Gaussian bands which simulate the CT absorption, from which the $\Delta\tilde{\nu}_{1/2}$ values can be extracted.[28] The coupling parameters for dyads **1** and **2** are then calculated from eq 1, and these are summarized in Tables 1 and 2. It is interesting to notice that, despite the large difference in the optical energies of the CT bands, the coupling strength parameters H_{AB} are almost the same for both dyads, with mean

(30) (a) Marcus, R. A.; Siders, P. *J. Phys. Chem.* **1982**, *86*, 622. (b) Marcus, R. A.; Sutin, N. *Inorg. Chem.* **1975**, *14*, 213. (c) Sutin, N. *J. Photochem.* **1979**, *10*, 19. (d) Marcus, R. A. *J. Phys. Chem.* **1965**, *43*, 679−701. (e) Marcus, R. A. *Angew. Chem., Int. Ed.* **1956**, *24*, 966.

(31) (a) Hush, N. S. *Prog. Inorg. Chem.* **1967**, *8*, 391. (b) Hush, N. S. *Coord. Chem. Rev.* **1985**, *64*, 135. (c) Hush, N. S. *Electrochim. Acta* **1968**, *13*, 1005. (d) Mulliken, R. S. *J. Am. Chem. Soc.* **1952**, *64*, 811. (e) Mulliken, R. S.; Person, W. B. *Molecular Complexes*; Wiley: New York, 1969.

(32) Asymmetry in the band shape of Class II systems mostly arises from additional contributions of transitions from low-lying vibrational levels. An exact band shape analysis affords a quantum mechanical treatment (Franck−Condon analysis), which is ongoing work in our research group; see ref 38.

(33) (a) Day, P. *Endeavour* **1970**, *29*, 45. (b) Robin, M.; Day, P. *Adv. Inorg. Radiochem.* **1967**, *10*, 247.

values of 456 ± 20 and 441 ± 13 cm^{-1} for **1** and **2**, respectively. This result is not surprising, taking into account the similar geometries of the two compounds. This value is also analogous to the value of H_{AB} for a vinyl group in other studies. We also observed a weak but systematic dependence of the coupling parameter H_{AB} with the solvent, finding stronger couplings for more polar solvents. Since H_{AB} depends directly on the orbital overlap of the bridge and the donor and acceptor moieties, such behavior may be ascribed to slight variations in the geometry of the compounds.

3. Solvent Dependence of the IET Process. Marcus theory allows correlating the energy of an optical absorption due to a CT transition (E_{opt} or $h\tilde{\nu}_{max}$) with the free energy changes that the molecule experiences during the charge separation and recombination resulting from the internal bond length alterations (or vibrational changes), λ_v, and the outer solvent reorganizations, λ_o. For asymmetric compounds, an additional term, $\Delta G°$, named redox or energetic asymmetry, describing the energy difference between the charge-separated D^+A^- state and the neutral DA ground state, is added (see Scheme 2), so that the total energy balance is expressed as follows:

$$E_{opt} = h\nu_{max} = \lambda_v + \lambda_o + \Delta G° \qquad (2)$$

The solvent dependence of the optical energy of the CT band enters into this formula in two different ways: one is by the outer solvent reorganization energy, but it also plays a role through the redox asymmetry term, while the internal (vibrational) reorganization energy is supposed not to vary with the solvent.

A common way to describe the polarity of a solvent is by the *dielectric continuum theory*, where the solvent is modeled as a structureless continuum and its properties are defined only by the physically observable static and optical dielectric constants ϵ and n^2 (with refractive index n). Depending on the geometrical model chosen, the solvent dependence of the individual energies can then be described by solvent polarity functions consisting of different combinations of ϵ and n^2.[34] For a dipole in a spherical cavity (i.e., the point dipole in a dielectric continuum), the solvent dependences of the energy of the optical transition E_{opt}, the redox asymmetry $\Delta G°$, and the solvent reorganization energy λ_o can be related to the polarity functions $f(\epsilon)$ and $f(n^2)$ by the following equations (in SI units):[35−37,38a]

$$E_{opt} = E_{opt(vacuum)} - \frac{1}{4\pi\,\epsilon_0\,a_0^3}[2\vec{\mu}_g(\vec{\mu}_e - \vec{\mu}_g)(f(\epsilon) - f(n^2)) + (\vec{\mu}_e^{\,2} - \vec{\mu}_g^{\,2})\,f(n^2)] \qquad (3)$$

$$\lambda_{o(\epsilon,n)} = \frac{1}{4\pi\,\epsilon_0\,a_0^3}(\vec{\mu}_e - \vec{\mu}_g)^2(f(\epsilon) - f(n^2)) \qquad (4)$$

$$\Delta G°_{(\epsilon)} = \Delta G°_{(vacuum)} - \frac{1}{4\pi\,\epsilon_0\,a_0^3}(\vec{\mu}_e^{\,2} - \vec{\mu}_g^{\,2})\,f(\epsilon) \qquad (5)$$

where the functions $4(x)$ are equal to $(x - 1)/(2x + 1)$, with $x = \epsilon$ or n^2. μ_e and μ_g are respectively the dipole moments of the excited and the ground states, and a_0 is the effective spherical radius of the donor−acceptor dyad, which can be calculated by $a_0 = (3M/4\pi\rho N_A)^{1/3}$, with M the molar mass, N_A Avogadro's number, and ρ the density of the given donor−acceptor dyad molecule (obtained from crystallographic data).[39] $\Delta G°_{(vacuum)}$ is the free energy difference between the D^+A^- excited state and the DA ground state in a vacuum.

Taking into account the solvent continuum model and according to eq 3, there must be a linear relationship between the position of the CT absorption maximum, E_{opt}, and the solvent polarity. From a multiple regression analysis of E_{opt}, estimates for the ground- and the excited-state dipole moments can be obtained. Furthermore, this analysis provides us with a value for the optical energy of the CT transition in the absence of any solvent influence, $E_{opt(vacuum)}$, where λ_o is zero. The multiple regression linear fit for compound **1** gives $E_{opt} = 13.11(\pm0.39) - 1.97(\pm0.36)\cdot(f(\epsilon) - f(n^2)) - 11.10(\pm1.78)\cdot f(n^2)$ [1000 cm^{-1}], with R(error) = 0.74 and sd = ±0.17. For compound **2**, $E_{opt} = 9.80(\pm0.60) - 2.32(\pm0.56)\cdot(f(\epsilon) - f(n^2)) - 13.6(\pm2.76)\cdot f(n^2)$ [1000 cm^{-1}], with R(error) = 0.75 and sd = ±0.22. The dipole moments of the ground and excited states are then calculated to be $\mu_g = 2.2 \pm 0.8$ and 2.5 ± 0.9 D and $\mu_e = 22.8 \pm 2.0$ and 26.6 ± 2.9 D for compounds **1** and **2**, respectively. It can be seen that the dipole moments of ground states for both compounds are very small and almost equal, while the dipole moments of the excited states are slightly larger for compound **2**, which explains the higher sensitivity of E_{opt} to solvent polarity changes. The difference between μ_e and μ_g ($\Delta\mu_{eg}$) then allows us to estimate the adiabatic CT distances to be 5.0 ± 0.8 and 5.4 ± 0.9 Å for compounds **1** and **2**, respectively. For the above-described multiple regression analysis, rather rough linear relationships were obtained, with some deviations from linearity. A closer look at Tables 1 and 2 reveals that the IET energies found for compound **2** in aromatic and oxygen-containing solvents are generally lower than expected from the linear fit obtained with the solvent continuum model, while for *n*-hexane and chlorinated aliphatic solvents the IET energies exhibit a positive deviation from the linear fit. The same trend is observed for compound **1**. Clearly, this result shows that there are some specific solvent/solute interactions present in both systems for which the solvent continuum model, or other models further elucidated[40] which only take into account the solvent polarity, are only an approximate description.

In order to take into account such specific interactions and to explain in more detail the solvatochromic behaviors, several empirical methods have been developed.[41,42] From them we have used the most extended one, the so-called linear solvation energy

(34) (a) Brunschwig, B. S.; Ehrenson, S.; Sutin, N. *J. Phys. Chem.* **1987**, *91*, 4714. (b) Karelson, M. M.; Zerner, M. C. *J. Phys. Chem.* **1992**, *96*, 6949.
(35) Zoon, P. D.; Brouwer, A. M. *ChemPhysChem.* **2005**, *6*, 1574.
(36) (a) Lippert, E. *Z. Electrochem.* **1957**, *61*, 962−975. (b) Mataga, N.; Kaifu, Y.; Moizumi, M. *Bull. Chem. Soc. Jpn.* **1956**, *29*, 465−470.
(37) (a) Onsager, L. *J. Am. Chem. Soc.* **1936**, *58*, 1486−1493. (b) Kirkwood, J. G. *J. Chem. Phys.* **1934**, *2*, 351−361.
(38) (a) Cortés, J.; Heitele, H.; Jortner, J. *J. Phys. Chem.* **1994**, *98*, 2527−2536. (b) Gould, I. R.; Noukakis, D.; Gomez-Jahn, L.; Young, R. H.; Goodman, J. L.; Farid, S. *Chem. Phys.* **1993**, *176*, 439.
(39) With M(**1**) = 962 g/mol and M(**2**) = 1062 g/mol, and $\rho = 1.62$ g/cm^3, a_0 is calculated to be 6.17 and 6.38 Å for compounds **1** and **2**, respectively. The use of an effective spherical radius is a clear simplification in the case of the complex molecular geometries studied here.
(40) King, G.; Warshel, A. *J. Chem. Phys.* **1990**, *93*, 8682.
(41) (a) Katritzky, A. R.; Fara, D. C.; Yang, H.; Tämm, K. *Chem. Rev.* **2004**, *104*, 175. (b) Dong, J.; Solntsev, K. M.; Tolbert, L. M. *J. Am. Chem. Soc.* **2006**, *128*, 12038.
(42) (a) Kamlet, M. J.; Taft, R. W. *J. Am. Chem. Soc.* **1976**, *98*, 377. (b) Kamlet, M. J.; Abboud, J-L.; Taft, R. W. *Prog. Phys. Org. Chem.* **1981**, *13*, 481. (c) Laurence, C.; Nicolet, P.; Dalati, M. T.; Abboud, J.-L. M.; Notario, R. *J. Phys. Chem.* **1994**, *98*, 5807−5816.

relationship (LSER) developed previously by Kamlet, Taft, and co-workers,[42−46] to better understand the solvatochromic behaviors of dyads **1** and **2**. As far as we know, this is the first time that a LSER method has been used for understanding the solvatochromic behavior of an IET process. The LSER treatment is a powerful tool for the study of the principal intermolecular interactions that control a specific physicochemical process in solution. The LSER assumes that the changes in the free energy associated with a physicochemical process are the sum of different independent contributions generated from the different solvent/solute interactions, which can be categorized in two groups: the exoergic and endoergic interactions.[42] The exoergic interactions have their origins in attractive solute/solvent interactions and can be quantified by the solvatochromic parameters π^*,[43] α,[44] and β.[45] These parameters can be classified as nonspecific (π^*) and specific (α and β) ones. The π^* parameter measures the exoergic effects of dipole/dipole and dipole/induced dipole interactions between the solute and the solvent molecules; e.g., it is a measure for the dipolarity/polarizability. For some processes and when several solvents are used at the same time, a corrector term δ for the parameter π^* must be added in order to have the correct polarizability for all solvents at the same time.[46,47] The solvatochromic parameter β is a quantitative empirical measure of the ability of a solvent to act as hydrogen-bond acceptor (or electron donor) toward a standard solute; i.e., it is a measure for the basicity of the solvent. By contrast, the empirical parameter α measures quantitatively the ability of a solvent to act as a hydrogen-bond donor (or electron-pair acceptor for acidity of the solvent) toward a standard solute. Finally, we have to consider the endoergic term Ω, named the cohesiveness term.[48,49] This term measures the work required for separating the solvent molecules to provide a suitably sized and shaped enclosure in which the solute molecule can be accommodated. The Ω term represents the physical quantity of cohesive pressure—or cohesive energy density—of the solvent. Therefore, the generalized LSER equation that describes the IET energy associated with the CT absorption for a donor−acceptor dyad in any solvent media adopts the form of eq 6,

$$\tilde{\nu}_i = \tilde{\nu}_i^{\circ} + a_i\,\alpha + b_i\,\beta + s_i\,[\pi^* + d_i\,(\delta)] + m_i\,\Omega \qquad (6)$$

where the coefficients s_i, d_i, a_i, b_i, and m_i and the constant $\tilde{\nu}_i^{\circ}$ are characteristic of each studied compound i, being independent of the nature of the solvent. These coefficients are indicative of the sensitivity of the IET process exhibited by the compound i toward variation of each solvent property (π^*, α, β, δ, and Ω). Such coefficients must have negative (or positive) signs according to the endoergic (or exoergic) nature of each term, and the independent term $\tilde{\nu}_i^{\circ}$ (in cm^{-1}) is the energy of the absorption expected for the IET process in the absence of a solvent, i.e., in a vacuum.

The energies of the CT bands have been measured for dyads **1** and **2** at room temperature in different solvents (see Table S1), which were chosen as representative of the 11 groups in which the most common laboratory solvents have been classified.[50] Due to the distinct solubilities of the two dyads, only 22 and 17 solvents of 8 different groups were used for **1** and **2**, respectively, in their corresponding LSER treatments.[51] By fitting the experimental data $\tilde{\nu}_i$ (cm^{-1}) obtained in different solvents with the known π^*, α, β, δ, and Ω parameters, summarized in Table S1, to eq 6 through a multivariable linear regression, we have calculated the coefficients s_i, d_i, a_i, b, and m_i and the independent term $\tilde{\nu}_i^{\circ}$, corresponding to the IET process in any solvent media for compounds **1** and **2**.[52] By mean of a statistical analysis, those coefficients with a low significance level were removed from the calculated models. The final LSER models for dyads **1** and **2** are those described by eqs 7 and 8, respectively, which include only the specific solute/solvent interaction terms of H-bonding and the dipolarity/polarizability terms that contribute significantly to the solvent-induced IET process.

$$\tilde{\nu}_i = 11.12(\pm 0.05)_i + 1.10(\pm 0.23)\alpha - 0.76(\pm 0.12)\beta - 0.52(\pm 0.10)[\pi^* - 0.36_i(\pm 0.07)(\delta)] \qquad (7)$$

$$\tilde{\nu}_i = 7.28(\pm 0.04)_i + 2.68(\pm 0.43)\alpha - 0.54(\pm 0.16)\beta - 0.88(\pm 0.12)[\pi^* - 0.27(\pm 0.08)(\delta)] \qquad (8)$$

Table S2 lists the resulting regression coefficients and the statistical information of the multivariable linear regressions. Figure 3 shows the good agreement achieved between the calculated energies from the LSER models (eqs 7 and 8) and the experimental data for dyads **1** and **2**.[53,54]

Finally, from the analysis of the LSER models, the following information can be extracted: (a) The IET energy for dyads **1** and **2** is not only sensitive to the polarity of the solvent but also very sensitive to changes of the H-bond donor ability of the surrounding media. Thus, a positive value of the coefficient a_i results in an increase in the energy (a blue-shift of the band) of the IET band with increasing solvent H-bond donor ability. This fact may be explained in terms of a relative stabilization of the DA ground state with respect the D^+A^- excited state in the presence of H-bond-donating solvents due to specific

(43) (a) Taft, R. W.; Kamlet, M. J.; Abboud, J.-L. M. *J. Am. Chem. Soc.* **1977**, *99*, 6027. (b) Abboud, J.-L. M.; Notario, R. *Pure Appl. Chem*. **1999**, 71, 645−718.
(44) Taft, R. W.; Kamlet, M. J. *J. Am. Chem. Soc.* **1976**, *98*, 2886.
(45) Marcus, Y. *Chem. Soc. Rev*. **1993**, *22*, 409−416.
(46) Taft, R. W.; Kamlet, M. J.; Abboud, J.-L. M. *J. Am. Chem. Soc.* **1981**, *103*, 1080.
(47) Usually the following values are used for such corrector parameter: $\delta = 0.0$ for non-chlorinated aliphatic solvents, $\delta = 0.5$ for polychlorinated aliphatic solvents, and $\delta = 1$ for aromatic solvents.
(48) (a) Langmuir, I. *Third Colloid Symposium Monograph*; Chemical Catalog Co.: New York, 1925; p 3. (b) Amidon, G. L.; Yalkowsky, S. H.; Anik, S. Y.; Valvani, S. C. *J. Phys. Chem.* **1975**, *79*, 2239. (c) Hall, G. G.; Smith, C. M. *J. Mol. Struct. (THEOCHEM)* **1988**, *179*, 293. (d) Herman, R. B. *J. Phys. Chem.* **1972**, *76*, 2754. (e) Silla, E.; Tuñon, I.; Villar, F.; Pascual-Ahuir, J. L. *J. Mol. Struct. (THEOCHEM)* **1992**, *86*, 369.
(49) Hildebrand, J. H.; Scott, R. L. *The solubility of Non-Electrolytes*, 3rd ed.; Dover Publications: New York, 1964; p 424.
(50) Ventosa, N.; Ruiz-Molina, D.; Sedó, J.; Rovira, C.; Tmas, S.; André, J.-J.; Bibier, A.; Veciana, J. *Chem. Eur. J.* **1999**, *5*, 3533−3548.
(51) Two solvents were discarded in the LSER treatments of dyads **1** and **2** given in Table S1, since they do not follow the general trends of other solvents, probably because of the presence of impurities; see ref 52.
(52) For the calculations, we have used α, β, and π^* parameters from ref 45 since they were derived under the same conditions. Despite using parameters from different sources for the multiple regression analysis, very similar results have been obtained.
(53) (a) *SYSTAT for Windows*, Version 5; SYSTAT, Inc.: Evanston, IL, 1992. (b) Neter, J.; Wasserman, W.; Kunter, M.*Applied linear statistical models*, 2nd ed.; Richard E. Irwin, Inc.: Homewood, IL, 1985. (c) Velleman, P. F.; Welsh, R. E. *The Americal Statistician* **1981**, *35*, 234.
(54) By performing a coefficient analysis of each independent variable, we saw that some of the solvents could be left out of the analysis. From the plotting of the experimental values versus the calculated values, we also found that there were some solvents that do not follow the regression model. After those solvents were eliminated, the resulting fits were much better. For the new fits, the linear regression model was valid, with a significance superior—$F = 47$, $p(0.0001)$—obtained in first place. The fit is robust because the sign of each coefficient is maintained for all the different fits considering all solvents.

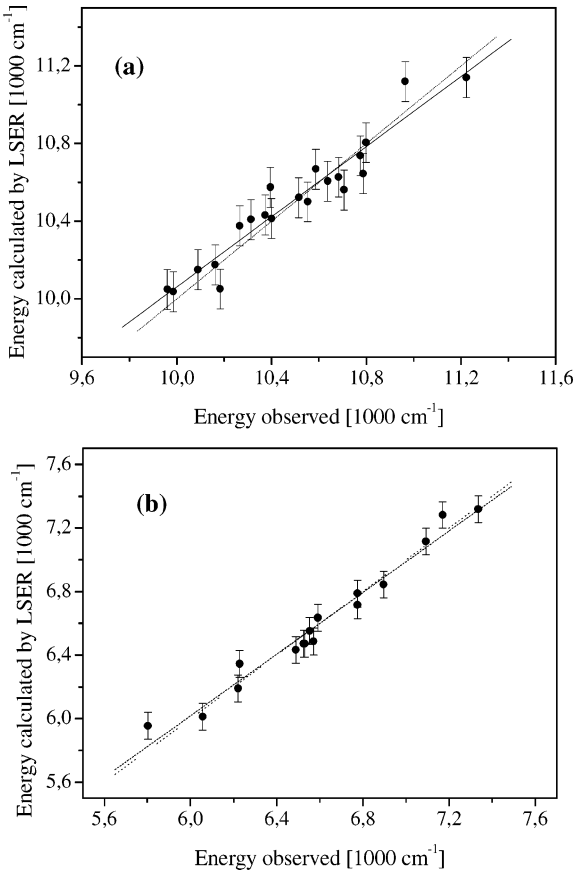

Figure 3. IET energies, calculated using the LSER eqs 7 and 8, versus the experimentally observed values (solid lines correspond to the best multivariable linear regressions and dashed lines to an ideal accordance) for dyads (a) **1** and (b) **2**.

interactions of the solvent. The processes of solvation of the electronegative PTM unit in the neutral DA ground state and in the D^+A^- state are very similar due to the fact that in both cases the charge is effectively delocalized over the three large phenyl groups substituted by five chlorine atoms, a situation that does not produce any preferential stabilization. Moreover, the sterically hindered propeller morphology of the PTM unit does not seem to help for a specific solvent interaction. On the other hand, the negative charge on each cyclopentadienyl ring of the ferrocene unit in the DA ground state is much more accessible and localized than in the ferricinium unit of the charge-separated D^+A^- state because in the latter case the charge is counterbalanced by the additional positive charge on the Fe (III). Therefore, these differential characteristics may produce a preferential stabilization of the neutral ground state with H-bond-donating solvents. (b) The fact that the coefficient a_i is higher for dyad **2** than for **1** means that the former dyad is more sensitive to the solvent H-bond donor ability. Probably, the stabilization of the DA ground state of **2** is higher than that of **1** because it has the ferrocene unit substituted by nine electron-donating methyl groups, which give to the cyclopentadienyl (Cp) rings much more negative charge to be stabilized by the solvent. (c) The sign of the coefficient b_i is negative, indicating that an increase in the solvent electron donor ability decreases the energy of the IET, which can be explained in terms of a pronounced stabilization of the D^+A^- excited state due to specific interactions of the solvent with the ferrocenium unit. (d) The fact that the coefficient b_i is much higher for **1** than for **2** is indicative that the effect is stronger for the *non*-methylated ferrocene dyad **1**, most probably due to the lower sterical shielding of the electron-accepting iron atom by the two Cp rings compared to the nonamethylated one and also due to the less effective positively charged ferrocenium of **2**, also due to the electron-donating methyl groups. (e) The sign of the coefficient s_i is negative for both compounds, showing that an increase in the solvent polarity decreases the energy of the IET, increasing the wavelength (red-shift) of the band (see Figure 2). This fact indicates that a stabilization of the D^+A^- excited state is present in more polar solvents. (f) The IET process for compound **2** is more sensitive to polarity changes than that for **1**, in accordance with the slightly higher dipolar moment found for compound **2**. (g) The IET processes studied are not sensitive to the solvent cohesiveness parameter, Ω.

In conclusion, the LSER model accounts for the energy of the IET process for compounds **1** and **2** in different solvents with more accuracy than the solvent continuum model alone because specific solvent/solute interactions are taken into account. It is clearly observed that solute/solvent interactions are dependent not only on the polarity of the solvent and its capacity to undergo $\pi-\pi$ interactions with the solute to stabilize the charge-separated excited state, but also on the H-bond donor ability of the solvent or the H-bond acceptor ability, resulting in either an increase or a decrease of the IET energy. Indeed, it is possible to fine-tune the energy of the IET by carefully selecting the appropriate solvent.

4. Normal and Inverted Marcus Regions. As it has been explained before, the classical solvent continuum model fails to give a complete description of the solvent dependence of the IET energies due to the presence of specific solvent/solute interactions. However, even if the relationship with the solvent polarity functions is not perfect, the classical model shows the expected trends, finding lower IET energies for larger solvent polarities. Additionally, it provides a description of the solvent dependence of the outer-sphere reorganization energy, λ_o, and the redox asymmetry, $\Delta G°$, by means of eqs 4 and 5. However, to estimate values for the internal reorganization energy in a total energy balance according to eq 2, it is necessary to estimate first the redox asymmetry in a vacuum, $\Delta G°_{(vacuum)}$. We can determine such asymmetric energies from a solvent electrochemical study. Then, according to eq 2, it will be possible to establish a total energy balance and determine the relative importance of each energy term in a given solvent.

The change in the free energy, $\Delta G°$, associated with the IET can be estimated by using electrochemical data since the redox asymmetry between the DA ground state and the D^+A^- charge-separated state is related to the difference between the electrochemical oxidation and reduction potentials of the donor and acceptor moieties; i.e., $\Delta E_{1/2} = E_{ox}(D) - E_{red}(A)$ plus a term that takes into account the influence of two opposite charges. Of course, electrochemical measurements are always limited by the poor solubility of the electrolyte in nonpolar solvents, and therefore the experimentally obtained free energy changes are restricted only to polar solvents.[55] It is well known that substituted PTM radicals and ferrocenes undergo clean, reversible one-electron redox reactions. Thus, in the cyclic voltammograms (CV) of radicals **1** and **2**, only one reduction process was observed, which is assigned to the reduction of the PTM

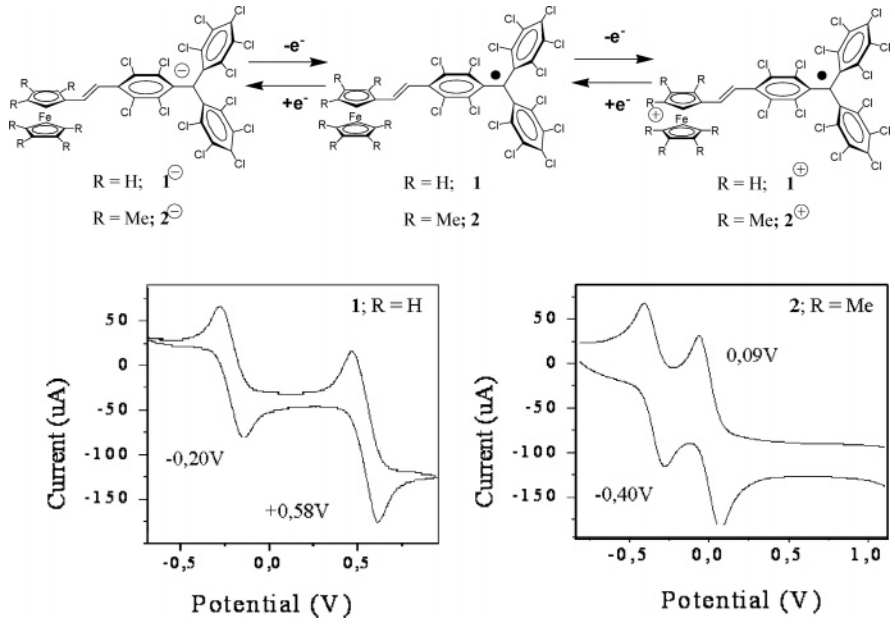

Figure 4. (Top) Redox process associated with the first oxidation and first reduction potentials of compounds **1** and **2**. (Bottom) Cyclic voltammograms of radicals **1** and **2** in dichloromethane using (TBA)PF_6 (0.1 M) as electrolyte.

Table 3. Experimental Electrochemical Redox Potentials [in V] and Corrected Free Energies $\Delta G°$ [1000 cm^{-1}] Calculated According to Eq 9 for Radicals **1** and **2** with Different Charge-Transfer Distances r_{DA} in Different Solvents

				$\Delta G°$		
solvent	$\Delta E_{1/2\,red}$[a] PTM/PTM^-	$\Delta E_{1/2\,ox}$[a] Fc/Fc^+	ΔE_{redox}	r_{DA} = 9.5 Å[b] r_{DA} = 9.7 Å[c]	r_{DA} = 6 Å	r_{DA} = 5 Å
			Compound **1**			
$CHCl_3$	−0.809	0.067	0.876	6.57[b]	5.92	5.51
CH_2Cl_2	−0.637	0.127	0.764	5.82[b]	5.40	5.14
PhCN	−0.553	0.076	0.629	4.87[b]	4.65	4.53
acetone	−0.485	0.082	0.567	4.38[b]	4.15	4.02
MeCN	−0.489	0.087	0.576	4.51[b]	4.37	4.29
linear fits of $\Delta G°$ vs solvent polarity function $f(\epsilon)$[d]:		intercept		13.1 (1.32)	10.9 (1.28)	9.57 (1.26)
		slope		−17.9 (2.99)	−13.8 (2.93)	−11.1 (2.85)
		regression coefficient *R*		−0.96	−0.94	−0.91
		standard deviation *S*		0.30	0.29	0.29
			Compound **2**			
$CHCl_3$	−0.866	−0.392	0.474	3.33[c]	2.68	2.26
THF	−0.63	−0.283	0.347	2.42[c]	1.94	1.65
CH_2Cl_2	−0.698	−0.373	0.325	2.28[c]	1.86	1.60
PhCN	−0.558	−0.353	0.205	1.45[c]	1.23	1.11
acetone	−0.484	−0.315	0.169	1.17[c]	0.94	0.81
linear fits of $\Delta G°$ vs solvent polarity function $f(\epsilon)$[d]:		intercept		9.90 (0.79)	7.81 (0.75)	6.45 (0.73)
		slope		−18.3 (1.84)	−14.3 (1.75)	−11.7 (1.72)
		regression coefficient *R*		−0.98	−0.98	−0.97
		standard deviation *S*		0.17	0.16	0.16

[a] Potentials are referred vs Fc/Fc^+ as internal standard. [b] Crystallographically determined charge-transfer distance for compound **1**: r_{DA} = 9.5 Å. [c] Crystallographically determined charge-transfer distance for compound **2**: r_{DA} = 9.7 Å. [d] Linear fit: $\Delta G°(r_{DA})$ = intercept − slope*$f(\epsilon)$; *R*-value and standard deviation. Resulting absolute errors were ± 5 mV for ΔE_{redox} and ± 50 cm^{-1} for $\Delta G°$.

moiety. For both compounds **1** and **2**, these reduction potentials are observed between −0.45 and −0.85 V (vs Fc/Fc^+), depending on the solvent used. Both compounds also exhibit one-electron reversible oxidation waves which can be assigned to the oxidation of the Fe(II) to Fe(III) of ferrocene moieties. As expected, the ferrocene moiety in radical **2** is much more easily oxidized than **1**, by about 0.4 V, due to the nine additional electron-donating methyl groups of the Cp rings (see Figure 4).

In order to determine the influence of solvents in changing the free energy associated with the IET, we have performed CV experiments for radicals **1** and **2** in five different solvents covering the polarity range from moderately polar ($CHCl_3$) to very polar (acetonitrile) (Table 3). As shown in Figure 5, there is a good linear relationship between the $\Delta E_{1/2}$ values of radicals and the solvent polarity function $f(\epsilon)$, as expected from eq 5. Thus, for radicals **1** and **2**, lower potential differences are found in more polar solvents, showing in addition an interesting parallel solvent polarity dependence with a 0.41 V higher

(55) Generally, in the optical spectra of the studied compounds in solvents containing an electrolyte, a weak blue-shift of the CT absorption by about 50 cm^{-1} is found with respect to the optical data obtained in electrolyte-free solvents, probably due to ion-pairing effects. Since such small deviations are within the experimental error, the optical energies E_{opt} are assumed to be the same under both conditions.

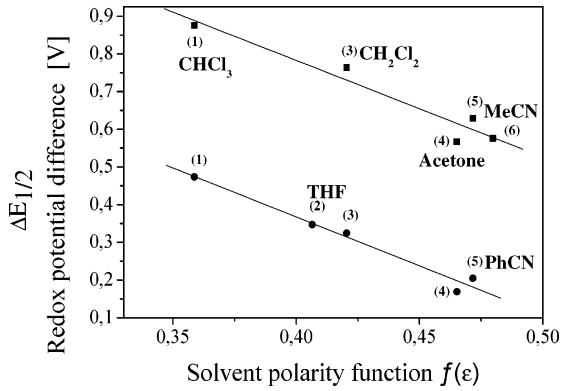

Figure 5. Plots of the redox potential differences between donor oxidation and acceptor reduction potentials found for radicals **1** (black squares) and **2** (red points) versus the solvent polarity function $f(\epsilon)$. Straight lines represent the best fit from a linear regression analysis.

potential difference for radical **1**. This fact reflects the reduced donor strength of the ferrocene unit with respect to the nonamethylated ferrocene unit of radical **2**.

The above-described electrochemical data are obtained for the donor (ferrocene) or acceptor (PTM) moieties without the presence of a negative or positive charge in their vicinity; therefore, they do not provide us directly with the redox asymmetry. To account for the influence of a charge residing in the proximity of the given donor or acceptor in the charge-separated state on the redox potentials, a Coulombic energy correction work term, w, has to be taken into account (see eq 9a). This correction work term can be calculated by using the Debye−Hückel expression, eqs 9b and 9c,[56] where the strength of the electrostatic interaction between the two charged moieties is modified by the ions of the electrolyte (all expressions are given in SI units).[57,58]

$$\Delta G^\circ = eN_L[E^{ox}_{1/2}(D) - E^{red}_{1/2}(A)] - w \tag{9a}$$

$$w = \frac{z_1 z_2 N_L e^2}{4\pi \epsilon_0 \epsilon_S r_{DA}(1 + r_{DA}\beta \sqrt{\mu})} \tag{9b}$$

$$\beta = \sqrt{\frac{2N_L e^2}{\epsilon_0 \epsilon_S k_B T}} \tag{9c}$$

In eq 9b, the expression $\beta\sqrt{\mu}$ is the inverse Debye length, a measure for the radius of the ion atmosphere formed by the electrolyte that surrounds the donor and acceptor moieties, which depends directly on the ion-strength μ of the solution. The static dielectric constant ϵ_S enters reciprocally, which makes the values for the work term larger in apolar solvents. Additionally, w is very sensitive to the CT distance r_{DA}. To account for a possibly smaller effective CT distance than that obtained from the crystallographic data for compounds **1** and **2**, we have also calculated the work term w and the redox asymmetries ΔG° for smaller distances r_{DA} than those determined from crystallographic data. Electrochemical data and values for the corrected redox asymmetries ΔG°, together with the results obtained from linear fits for $\Delta G^\circ(r_{DA})$ versus the solvent polarity function $f(\epsilon)$ from eq 5, are listed for both compounds in Table 3.

With the redox asymmetries, ΔG°, calculated from the electrochemical data for different CT distances, r_{DA}, it is possible to write an energy balance within the Marcus theory and to calculate the reorganization energies according to eq 2. An estimated value for λ_v can be obtained by extrapolating ΔG° as a function of the solvent polarity when $f(\epsilon)$ reaches zero and the solvent reorganization energy λ_o vanishes. Naturally, the results differ largely depending on the distinct $\Delta G^\circ(r_{DA})$ energies applied, since slopes of the linear fits of $\Delta G^\circ(r_{DA})$ versus $f(\epsilon)$ are less steep for smaller effective CT distances for both compounds. Only positive values for λ_v are physically reasonable, a condition which is not fulfilled for $\Delta G^\circ_{(vacuum)}$ values calculated with the crystallographically determined CT distances, since they exceed the maximum energy possible defined by E_{opt}.

On the other hand, with the dipole moments of the ground and the excited states already obtained from the multiple regression analysis of E_{opt}, we are able to calculate the expected slopes for ΔG° by using eq 5 in the dielectric continuum treatment to be $-11\,100 \pm 1780$ and $-13\,600 \pm 2760$ cm^{-1} for **1** and **2**, respectively. The best agreement between the expected and experimental slopes for $\Delta G^\circ(r_{DA})$ is found for compound **1** when an effective (diabatic) CT distance $r_{DA} = 5$ Å (slope $= -11\,100 \pm 2850$ cm^{-1}) is assumed and for compound **2** when $r_{DA} = 6$ Å (slope $-14\,300 \pm 1750$ cm^{-1}) is assumed. Thus, the internal reorganization energy for **1** under vacuum conditions is estimated to be $\lambda_v = 3550 \pm 1650$ cm^{-1}, which is much higher than that found for compound **2**, $\lambda_v = 1990 \pm 1350$ cm^{-1}. This interesting discrepancy may be explained by the influence of different molecular vibrational modes contributing to the reorganization energy in both compounds. Additionally, the total reorganization energy, $\lambda_v + \lambda_o$ in *n*-hexane is calculated to be $\lambda = 3720 \pm 1260$ and 2180 ± 750 cm^{-1} for **1** and **2**, respectively. As expected, these values do not differ too much from those obtained under vacuum conditions, implying that the solvent reorganization is very small in apolar solvents.

In Figure 6, the calculated energies together with the experimentally obtained optical energies are ploted versus the solvent polarity function $f(\epsilon)$ for compounds **1** and **2**.

It can be seen that for both compounds the solvent reorganization energy and the redox asymmetry exhibit opposite trends in their solvent dependence, as expected, with lower absolute values for λ_o and larger ones for $-\Delta G^\circ$ found in apolar solvents. But most important and very interesting is the fact that the absolute values of the solvent reorganization energy and the redox asymmetry are of the same order and linear fits of both cross each other in solvents of medium to high polarity. For solvents of low polarity, $-\Delta G^\circ$ exceeds the sum of both reorganization energies, while the opposite is true in high-polarity solvents. This fact is of utmost importance since it indicates a crossing of the so-called inverted and normal Marcus regions, where striking differences in the electron transport mechanisms between the donor and acceptor moieties are present. To the best of our knowledge, this is the first time that

(56) (a) Sutin, N. *Prog. Inorg. Chem.* **1983**, *30*, 441. (b) Debye, P. *Trans. Electrochem. Soc.* **1942**, *82*, 265.
(57) It has to be kept in mind that this equation was derived originally for a model describing a Coulombic interaction between isolated ions that are surrounded by a spherical ion atmosphere. Therefore, it can be only an approximation for more complicated organic molecules, where electron delocalization (resonance effects) may also be present. However, it has already been successfully applied for other covalently linked donor−acceptor molecules; see ref 58.
(58) Chen, P.; Mecklenburg, S. L.; Meyer, T. J. *J. Phys. Chem.* **1993**, *97*, 13126.

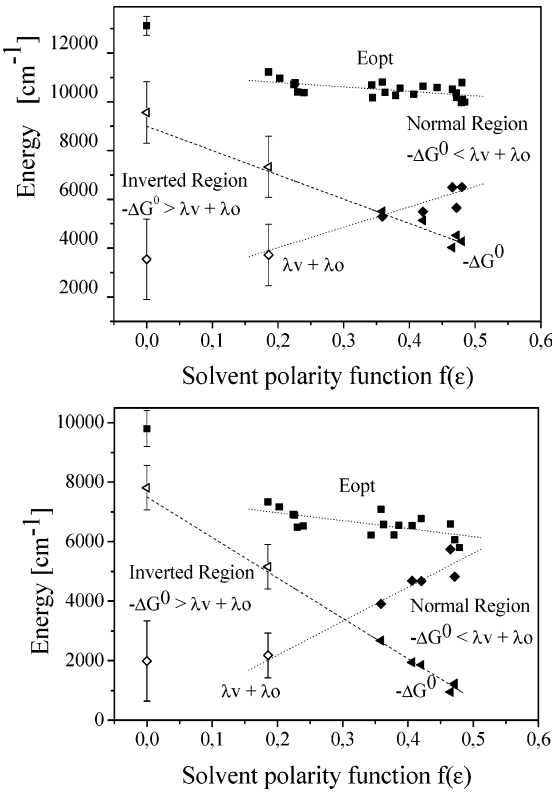

Figure 6. Total energy balance for (top) compound **1** with $r_{DA} = 5$ Å and (bottom) compound **2** with $r_{DA} = 6$ Å: ■, the experimental energy of the optical transition, E_{opt}; ◆, the sum $\lambda_o + \lambda_v$; and ▲, the asymmetric energy term $-\Delta G°$. Estimations of energy values for E_{opt}, $\Delta G°$, and λ_v under vacuum conditions ($f(\epsilon) = 0$) and in *n*-hexane ($f(\epsilon) = 0.18$) are obtained by extrapolation of experimental data and are indicated with closed symbols and error bars. Dashed and dotted lines represent expectations for energies within the dielectric continuum model.

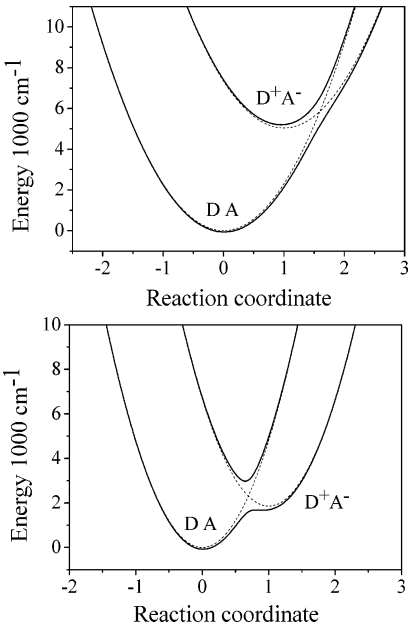

Figure 7. Diabatic (dashed line) and adiabatic (solid line) potential energy surface of the electronic ground state and the charge-separated state as a function of the electron-transfer coordinate for dyad **2**, calculated using quadratic functions λx^2 and $\lambda(1 - x)^2 + \Delta G°$ and the adiabatic energy surfaces according to ref 59 and eq 3. The energy values are obtained from Table 3 and derived according to eq 3 by extrapolation of the $\Delta G°$ values with the CT distance $r_{DA} = 6$ Å in *n*-hexane (top) and CH_2Cl_2 (bottom) using $\lambda = 2180$ cm^{-1}, $\Delta G° = 5160$ cm^{-1}, and $H_{AB} = 690$ cm^{-1} in *n*-hexane and $\lambda = 4910$ cm^{-1}, $\Delta G° = 1860$ cm^{-1}, and $H_{AB} = 710$ cm^{-1} in CH_2Cl_2.

such a change is reported for the same compound simply as a result of varying the solvent from apolar to polar. Such behavior is possible only because of the small redox splitting between the reduction and oxidation potentials of compounds **1** and **2**, where an excellent electron acceptor is combined with good and very good electron donors, respectively. Due to the smaller redox splitting, this effect is more pronounced in compound **2**.

With the calculated energies, it is possible to construct the diabatic energy surfaces with the two parabolic functions, λx^2 and $\lambda(1 - x^2) + \Delta G°$, and the adiabatic energy surfaces according eq 3 and ref 59, where $\lambda = \lambda_v + \lambda_o$ and x is the reaction coordinate. This is done, as an example, for compound **2** in hexane from the inverted region and in CH_2Cl_2 from the normal region and presented in Figure 7.[59]

5. Observation and Kinetics of Charge-Separated States of Dyads. To investigate the different CT kinetics present in the normal and inverted Marcus regions, fluorescence measurements are commonly applied if either the donor or the acceptor of dyads exhibits fluorescence. Fluorescence decay times can then be related to the rate of charge separation. Indeed, it is known that although nonconjugated PTM radicals are not very stable in front of white light, they show fluorescence, emitting in the visible spectral range around 600 nm. The photophysics of PTM radicals was studied extensively by Fox et al.,[60] and decay times on the nanosecond time scale were found, while in donor quenching experiments decay times were in the picosecond range, close to the diffusion-controlled limit. However, for dyads **1** and **2**, no fluorescence can be detected due to rapid intramolecular CT quenching. If the donor group is oxidized, the fluorescence is not recovered, since double bond isomerization can also cause effective quenching. As an alternative for fluorescence spectroscopy, CT kinetics can be investigated by transient absorption spectroscopy.

Picosecond time-resolved (or transient) absorption experiments provide a very powerful tool to study the intermediate states in a photoinduced reaction. Neither **1** nor **2** leads to transients detectable on a nanosecond time scale, probably because the excited state decays rapidly to the ground state. In order to investigate this in more detail, we have performed subpicosecond transient absorption measurements.[61] Time-resolved absorption experiments were performed for **1** and **2** with excitation at 390 nm, which corresponds to excitation of the PTM chromophore. Representative spectra at various delay times after the femtosecond excitation pulse are shown in Figures 8 and S2 for compounds **1** and **2**, respectively, in cyclohexane and butyronitrile. At very early times, a broad spectrum is observed and, very rapidly, the absorption around 700 nm decays, leaving a band around 550 nm. The time scale for this decay is ca. 200 fs, similar to the instrumental response time of our setup (Figure 8, top). The 700 nm band must be due to absorption of the initially produced PTM locally excited

(59) Brunschwig, B.; Creutz, C.; Sutin, N. *Chem. Soc. Rev.* **2002**, *31*, 168−184.

(60) (a) Fox, M. A.; Gaillard, E.; Chen, C.-C. *J. Am. Chem. Soc.* **1987**, *109*, 7088−7094. (b) Canepa, M.; Fox, M. A.; Whitesell, J. K. *J. Org. Chem.* **2001**, *66*, 3886−3892.

(61) (a) Aherne, D.; Tran, V.; Schwartz, J. *J. Phys. Chem. B* **2000**, *104*, 5382. (b) Matyoshov, D. V.; Landanyi, B. M. *J. Chem. Phys.* **1998**, *108*, 6362. (c) Brunschwig, B. S.; Ehrenson, S.; Sutin, N. *J. Phys. Chem.* **1986**, *90*, 3657.

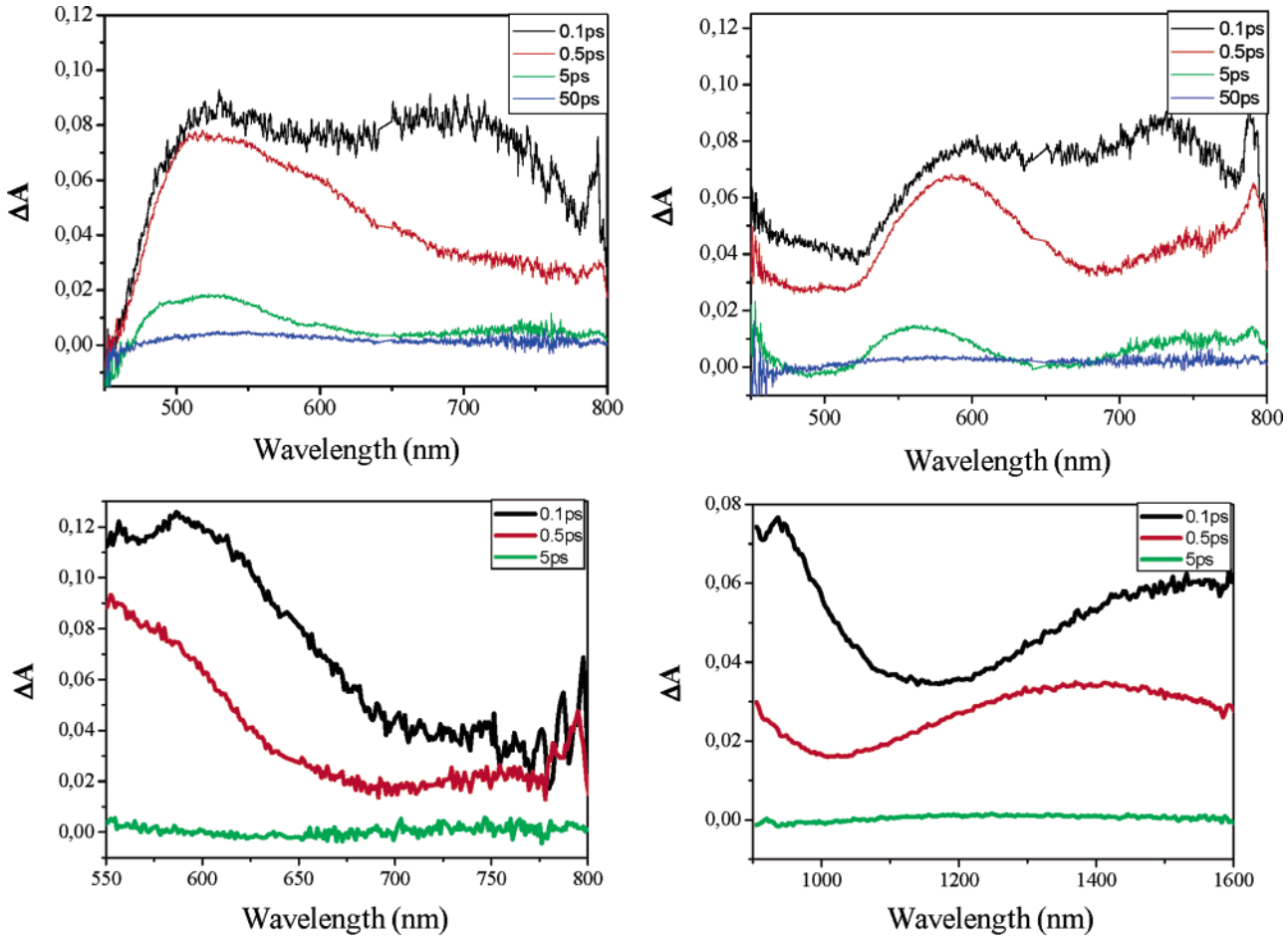

Figure 8. (Top) Transient absorption spectra of dyad **1** (right) and dyad **2** (left) in butyronitrile. (Bottom) Transient absorption spectra of dyad **1** in dichloromethane, excited at 936 nm, with two different detection systems: (left) vis range and (right) NIR range. These spectra were obtained in separate experiments, and their amplitudes cannot be directly compared.

state. The band around 550 nm should be attributed to the CT excited state, which can be described as $Fc^{+}-PTM^{-}$. The spectrum of the PTM anion chromophore, as obtained by chemical or electrochemical procedures in different derivatives, indeed shows a band in the same spectral range.

A more detailed account of the time decay constants for the different compounds in different solvents for these experiments is given in the Supporting Information.

For dyad **1** in dichloromethane, an experiment was performed with excitation at 936 nm, directly into the CT absorption band (Figure 8, bottom). In this case, a broad transient absorption band was detected in the 500−600 nm range, which decayed with a time constant of 0.7 ps, similar to what was found in *i*-Pr_2O and EtOAc with 390 nm excitation. Interestingly, we could also detect the transient absorption spectrum in the NIR range, which showed a band peaking at 1280 nm with a decay time of 0.7 ps. The almost identical decay times are consistent with the attribution of the vis and NIR bands to the same species, i.e., the CT excited state of **1**. Note that the 700 nm band that is seen in the experiments with UV excitation is not present in this case because the excitation directly populates the CT state. A more detailed account of this experiment is given in the Supporting Information.

The kinetics of the charge recombination step of the excited charge-separated $D^{+}A^{-}$ states have also been studied by picosecond transient absorption spectroscopy, revealing similar recombination rates around 10^{12} s^{-1} for both dyads with very small or null solvent dependences. Such ultrafast decay rates are in agreement with the barrierless regime of the Marcus model, which is consistent with the findings from the energy balance analysis.

Summary and Conclusions

The classical Marcus−Hush theory and the solvent continuum model, when applied to describe the large positive solvatochromism shown by dyads **1** and **2**, give a reasonable description of the experimental E_{opt} spectroscopic data in spite of the rigid assumptions made with this simple model. Deviations of the energies of optical absorption calculated with this simple model from the experimental E_{opt} values are due to the presence of specific solute/solvent interactions, as ascertained by a LSER treatment of the experimental spectroscopic data. Such a LSER treatment demonstrates the presence of specific H-bonding interactions between the dyad molecules and the solvents, along with nonspecific dipolarity/polarizabilty interactions that control, to different extents, the E_{opt} values. As far as we know, a LSER treatment has been never been used to explain and quantify the specific solute/solvent interactions that play a role in an IET process. From electrochemistry measurements in polar solvents, we have found that the energetic asymmetry, $\Delta G°$, between the donor and the acceptor units of the dyads shows a very good linear correlation with the solvent polarity function, $f(\epsilon)$,

indicating that the specific H-bonding interactions influence only the reorganization energy λ but not the energetic asymmetry $\Delta G°$. The large number of data obtained in different solvents, in conjunction with the Marcus−Hush theory and the solvent continuum model, allowed us to estimate the dipolar moments of the neutral ground state DA and of the excited charge-separated D^+A^- state for both dyads. The resulting dipolar moments show that the CT distances in both dyads are smaller than those determined from crystallographic data, probably because of the π-conjugation existing in both compounds. Stark spectroscopic experiments are in progress in order to confirm these values. Finally, the E_{opt} spectroscopic data and the redox asymmetry values $\Delta G°$ determined experimentally have allowed us to estimate, using the total energy balance $E_{opt} = \lambda + \Delta G°$, the reorganization energy, λ, and its solvent dependence. Since the resulting $\Delta G°$ and λ values are of the same order of magnitude but exhibit opposite trends in their solvent polarity dependence, a shift from the normal to the inverted Marcus regions with the solvent polarity is found. This is the first time that the mechanism of intramolecular electron transfer of a molecular system can be modified simply by changing its environment, which is of great interest in the field of molecular electronics. Picosecond transient absorption spectroscopy allowed us to observe and monitor, for the first time, the charge-separated states D^+A^- of dyads **1** and **2**, thereby unambiguously confirming the photoinduced electron transfer phenomena. The kinetics of the charge recombination step of the excited charge-separated D^+A^- states have also been studied by picosecond transient absorption spectroscopy, revealing similar recombination rates around 10^{12} s^{-1} for both dyads, with very small or null solvent dependences. Such ultrafast decay rates are in agreement with the barrierless regime of the Marcus model, which is consistent with the findings from the energy balance analysis.

Acknowledgment. This work was supported by the Ministerio de Educación y Ciencia, Spain (CONSOLIDER-C Project EMOCIONa; CTQ2006-06333/BQU), the Generalitat de Catalunya (2005 SGR-00591 and CERMAE), and The Netherlands Organization for the Advancement of Research (NWO). I.R. is grateful to the Ministerio Educación y Ciencia for a "Juan de la Cierva" contract, and C.S. thanks the program FWF Viena (Austria). We have appreciated the help of Michiel M. Groeneveld with the transient absorption experiments.

Supporting Information Available: Assignment of bands observed at 500 and 650 nm for dyads **1** and **2**, π-bridge-to-PTM acceptor CT transitions, LSER data, and transient absorption spectra of dyads **1** and **2**. This material is available free of charge via the Internet at http://pubs.acs.org.

JA066351G